The MACHO Project LMC Variable Star Inventory: XII. Three Cepheid Variables in Eclipsing Binaries

C. Alcock[1,2,3], R.A. Allsman[4], D.R. Alves[5], A.C. Becker[6,7], D.P. Bennett[8], K.H. Cook[1,2], A.J. Drake[1,9], K.C. Freeman[9], K. Griest[2,10], S.L. Hawley[6], S. Keller[1], M.J. Lehner[11], D. Lepischak[12], S.L. Marshall[1,2], D. Minniti[13], C.A. Nelson[1,14], B.A. Peterson[9], P. Popowski[15], M.R. Pratt[6,16], P.J. Quinn[17], A.W. Rodgers[9,18], N. Suntzeff[19], W. Sutherland[20], T. Vandehei[2,10], D.L. Welch[12]

(The MACHO Collaboration)

[1]Lawrence Livermore National Laboratory, Livermore, CA 94550
Email: kcook, adrake, keller19, stuart, cnelson@igpp.llnl.gov

[2]Center for Particle Astrophysics, University of California, Berkeley, CA 94720

[3]Department of Physics and Astronomy, University of Pennsylvania,
209 South 33rd St., Philadelphia, PA 19104-6396
Email: alcock@hep.upenn.edu

[4]Supercomputing Facility, Australian National University, Canberra, ACT 0200, Australia
Email: Robyn.Allsman@anu.edu.au

[5]Columbia Astrophysics Laboratory, 550 W. 120th St., NY, NY 10027
Email: alves@astro.columbia.edu

[6]Departments of Astronomy and Physics, University of Washington, Seattle, WA 98195
Email: hawley, pratt@astro.washington.edu

[7]Bell Laboratories, Lucent Technologies, 600 Mountain Avenue, Murray Hill, NJ 07974
Email: acbecker@physics.bell-labs.com

[8]Department of Physics, University of Notre Dame, IN 46556
Email: bennett@bustard.phys.nd.edu

[9]Research School of Astronomy and Astrophysics, Canberra, Weston Creek, ACT 2611, Australia
Email: kcf, peterson@mso.anu.edu.au

[10]Department of Physics, University of California, San Diego, CA 92093
Email: kgriest@ucsd.edu, vandehei@astrophys.ucsd.edu

[11]Department of Physics, University of Sheffield, Sheffield S3 7RH, UK
Email: m.lehner@sheffield.ac.uk

[12]McMaster University, Hamilton, Ontario Canada L8S 4M1
Email: lepischak, welch@physics.mcmaster.ca

[13]Depto. de Astronomia, P. Universidad Catolica, Casilla 104, Santiago 22, Chile
Email: dante@astro.puc.cl

[14]Department of Physics, University of California, Berkeley, CA 94720

[15]Max-Planck-Institut für Astrophysik, Karl-Schwarzschild-Str. 1, Postfach 1317, 85741 Garching bei München, Germany.
Email: popowski@mpa-garching.mpg.de

[16]Center for Space Research, Massachusetts Institute of Technology, Cambridge, MA 02139

[17]European Southern Observatory, Karl Schwarzchild Str. 2, D-8574 8 Gärching bel München, Germany
Email: pjq@eso.org

[18]Deceased.

[19]National Optical Astronomy Observatories,Cerro Tololo Inter-American Observatory, Casilla 603, La

ABSTRACT

We present a method for solving the lightcurve of an eclipsing binary system which contains a Cepheid variable as one of its components as well as the solutions for three eclipsing Cepheids in the Large Magellanic Cloud (LMC). A geometric model is constructed in which the component stars are assumed to be spherical and on circular orbits. The emergent system flux is computed as a function of time, with the intrinsic variations in temperature and radius of the Cepheid treated self-consistently. Fitting the adopted model to photometric observations, incorporating data from multiple bandpasses, yields a single parameter set best describing the system. This method is applied to three eclipsing Cepheid systems from the MACHO Project LMC database: MACHO ID's 6.6454.5, 78.6338.24 and 81.8997.87. A best-fit value is obtained for each system's orbital period and inclination and for the relative radius, color and limb-darkening coefficients of each star. Pulsation periods and parameterizations of the intrinsic color variations of the Cepheids are also obtained and the amplitude of the radial pulsation of each Cepheid is measured directly. The system 6.6454.5 is found to contain a 4.97-day Cepheid, which cannot be definitely classified as Type I or Type II, with an unexpectedly brighter companion. The system 78.6338.24 consists of a 17.7-day, W Vir Class Type II Cepheid with a smaller, dimmer companion. The system 81.8997.87 contains an intermediate-mass, 2.03-day overtone Cepheid with a dimmer, red giant secondary.

Subject headings: Magellanic Clouds — Cepheids — stars: AGB and post-AGB — stars: oscillations — binaries: eclipsing

1. INTRODUCTION

Large scale microlensing surveys have provided unprecedented resources for variable star research. Their long time baseline and stable, accurate photometry are ideal for the detection and analysis of such objects and the large number of systems observed increases the

Serena, Chile
Email: nsuntzeff@noao.edu

[20]Department of Physics, University of Oxford, Oxford OX1 3RH, U.K.
Email: w.sutherland@physics.ox.ac.uk

probability of finding astrophysically-interesting objects that either have escaped detection or do not exist in our own galaxy.

Very few regularly-pulsating stars are known to belong to eclipsing systems. One of the best studied is AB Cas, an Algol-type binary system, which contains a δ Scuti type primary (Rodríguez et al. 1998). Rodríguez & Breger (2001) list 6 additional δ Scutis which are members of eclipsing binaries. The lone Galactic candidate for an eclipsing binary containing a Cepheid variable was BM Cas (Thiessen 1956) but further study revealed that the variable was unlikely to be a Cepheid (Fernie & Evans 1997). The astrophysical benefits of a Cepheid variable in an eclipsing system could be considerable. If the system is double-lined, a determination of the Cepheid's luminosity and mass can be made that is not only more accurate than existing measurements but also truly independent of the intervening steps in the distance ladder. Such a system would provide the most direct measurement of the mass of a Cepheid and would offer an independent calibration of the period-luminosity relation.

Here we present the results of lightcurve analyses of three eclipsing Cepheid systems in the MACHO project Large Magellanic Cloud (LMC) database: MACHO ID's 6.6454.5, 78.6338.24 and 81.8997.87. In Sec. 2 we describe the sources of the photometric observations. Sec. 3 describes the model used to generate the lightcurve of an eclipsing Cepheid system and Sec. 4 describes the inverse problem of computing the parameters from an observed lightcurve. In Sec. 5 we present the results obtained for the three systems. Finally, Sec. 6 summarizes the analysis, describes work in progress and suggests future avenues for research.

2. OBSERVATIONS

Observations from several different sources are used in the analysis presented here but the majority are from the MACHO Project database. The MACHO observations were made with the refurbished 1.27m Great Melbourne Telescope at Mount Stromlo, near Canberra, ACT, Australia. It has been equipped with a prime focus reimager-corrector with an integral dichroic beamsplitter to give a 0.5 sq. deg field of view in two passbands simultaneously: a 450-590 nm MACHO V filter and a 590-780 nm MACHO R filter. These are each sampled with a 2×2 array of 2048×2048 Loral CCDs which are read out concurrently via two amplifiers per CCD in about 70 seconds. The resulting images cover 0.5 square degrees with 0.63 arcsec pixels (Alcock et al. 1995). Data reduction is performed automatically by Sodophot, a derivative of DoPhot (Schechter, Mateo, & Saha 1993). MACHO photometry is then transformed into Cousins V and R bands for further interpretation (Alcock et al. 1999). The eclipsing, pulsating nature of systems 6.6454.5 and 78.6338.24 was identified through

visual inspection of their lightcurves.

The eclipsing nature of 81.8997.87 was first reported by the Optical Gravitational Lensing Experiment (OGLE) project (Udalski et al. 1999) (OGLE ID LMC_SC16 119952) and the lightcurves for this system are a combination of observations in the OGLE and MACHO databases. OGLE observations were taken on the 1.3 m Warsaw telescope at Las Campanas Observatory, Chile operated by the Carnegie Institution of Washington. Photometry is in the standard BVI bands with the majority of the observations in the I band (Udalski et al. 1999). V and I measurements for 6.6454.5 (LMC_SC21 40876) have also been used here. The OGLE observations of the April 2000 eclipse of this system were graciously provided by Andrzej Udalski in advance of publication.

For the 1999 eclipse, observations of 6.6454.5 were taken by Nick Suntzeff from March 16 to April 21 on the 0.9m telescope at the Cerro Tololo Inter-American Observatory in Chile. The telescope is a 0.9-meter Ritchey-Chretien Cassegrain telescope with a dedicated 2048×2048 CCD detector. Observations were in standard BVI and were reduced by DAOPHOT, ALLSTAR and ALLFRAME.

A complete listing of the observations, from all sources, used in this paper is available at http://www.macho.mcmaster.ca/Data/EclCep/ecl_cep.htm. For guidance regarding form and content a partial listing is given in Tables 1 - 8.

3. MODEL

To analyse the lightcurve of eclipsing Cepheid systems, a geometric model based on classical equations (Binnendijk 1960, for instance) was developed. In this model the stars are assumed to be traveling on circular orbits. This isn't the most general case but may be appropriate here. It is found that two out of the three systems studied here have their primary and secondary minima separated by almost exactly one half period, consistent with a circular orbit. The stars themselves are treated as circular disks with radius (R) and central surface brightness ($J_\circ$). A linear limb-darkening law of the form

$$J = J_\circ(1 - x_\lambda + x_\lambda \cos(\gamma)), \tag{1}$$

is adopted where x_λ is the limb-darkening coefficient and γ is the angle between the surface normal at that point and the line of sight. Integrating over γ yields the light received from a non-eclipsed star as being proportional to

$$L = \pi R^2 J_\circ \left(1 - \frac{x_\lambda}{3}\right) \tag{2}$$

As absolute dimensions of the stars cannot be extracted from the lightcurve alone, the above parameters all represent ratios of observed quantities: the radii are measured in units of the orbital separation of the two stars, the surface brightnesses are normalized such that the mean light received outside of eclipse ($L_1 + L_2$) is 1.0.

In many programs the values of $J_\circ$ are modelled directly with a different value for each bandpass. As we have simultaneous MACHO V and R observations for all systems at all phases, we fit the colour, specifically the ratio J_V/J_R for each star, rather than the surface brightness. From this surface brightness ratio the usual $V-R$ colour index can be calculated. If I band observations are available, as they are for two of the three systems, the flux ratio J_V/J_I must also be defined, but is not used as a fitted parameter. Instead the $V-I$ colour index is computed from the $V-R$ colour using a linear relationship derived from the VRI observations of Cousins (1980) of a sample of southern stars. From the colour index, J_V/J_I can be calculated. To convert the surface brightness ratios into values for the individual surface brightnesses we employ the linear relationship between V surface brightness (J_V) and the $V-R$ colour index identified by Barnes, Evans, & Parsons (1976) (hereafter B-E). This relationship holds for stars of all spectral types and for all pulsational phases of the Cepheid. Unfortunately, it is not certain that the B-E relation applies to metal-poor Type II Cepheids and this is a potential source of systematic error in our results. However, not all Type II Cepheids are metal poor: one of the few Type II Cepheids known to be in spectroscopic binaries, the 2.4-day Type II Cepheid AU Peg (Harris, Olszewski, & Wallerstein 1984), has an [Fe/H] = +0.1. The B-E relation applies to Johnson filter definitions so the transformations of Bell & Gustafsson (1980) were used to convert to forms applicable to our Cousins bandpasses. With values of J_V the other surface brightnesses follow from the ratios.

The intrinsic variability of the Cepheids is handled by taking R and J_V/J_R as the minimum radius and the mean colour, respectively. Variability is then added to these values in some functional form. The colour variation is parameterized by a third-order Fourier series:

$$\Delta\left(\frac{J_V}{J_R}\right) = \sum_{k=1}^{3} A_k \cos(k\omega t) + B_k \sin(k\omega t) \tag{3}$$

The radial variation is modeled by the expression:

$$\Delta R = a\left|\sin\left(\frac{1}{2}\omega(t-t_\circ)\right)\right| \tag{4}$$

This produces a curve which, despite its discontinuity at $\Delta R = 0$, reproduces the broad features of the radial variation curve.

During eclipses, the decrease in the amount of light received from the system is calculated analytically, based on the radii of two overlapping discs and geometrical considerations

(Binnendijk 1960). The apparent separation of the centres of the two stars is given by

$$\delta^2 = \cos^2 i + \sin^2 i \ \sin^2 \theta \tag{5}$$

Whether the system is in eclipse or not is determined by comparing this distance to the instantaneous radii of the stars. Within eclipse, the area obscured by the eclipsing star is given by

$$Area = \frac{1}{2}R_1^2\left(2\alpha_1 - \sin(2\alpha_1)\right) + \frac{1}{2}R_2^2\left(2\alpha_2 - \sin(2\alpha_2)\right) \tag{6}$$

$$\cos(\alpha_1) = \frac{R_1^2 - R_2^2 + \delta^2}{2R_1\delta} \tag{7}$$

$$\cos(\alpha_2) = \frac{R_2^2 - R_1^2 + \delta^2}{2R_2\delta} \tag{8}$$

Multiplying the area by the surface brightness of the eclipsed star gives the decrease in flux.

The effects of limb-darkening within the eclipses are included by dividing the stellar disk into 100 concentric rings in a manner similar to Nelson & Davis (1972). A surface brightness is then assigned to each ring based on equation 1. The total light received from each star can then be calculated by computing the contribution from each ring and integrating over all of the rings. Within eclipses the integration must be performed within suitable limits based on the amount of each stellar surface that is visible. In practice, it is faster to compute the normal fluxes from equation 2 and then calculate the amount of flux lost based on the eclipse geometry. This is done by using equations 6-8 repeatedly for eclipsed stars of varying radii, which correspond to the rings into which the stellar disk is divided, and then summing over the total number of rings. So the flux lost would be given by

$$\sum_{i=0}^{100} J_i\left(Area(r_i) - Area(r_{i-1})\right) \tag{9}$$

where r_0 to r_{100} are the radii of individual rings ranging from 0 to the radius of the eclipsed star (R_1), $Area(r_i)$ is the area of a disk of radius r_i covered by the eclipsing star, given by equations 6-8, and J_i is the surface brightness of that ring given by equation 1. This flux lost is then subtracted from the flux given by equation 2 to give the eclipsed star's contribution to the sytem flux. Integration over the eclipsed region would be more accurate in principle, but poses the practical problem of being more difficult to implement. The limits of integration are particularly difficult to express for a star of varying radius as R_1 (as well as $J_\circ$ in equation 1) will be a function of time. Summation is more straightforward to implement and the loss of accuracy in the final flux value is, with the number of annuli being used, on the order of one part in 1000, as determined by comparison of trial summations over a full, uneclipsed disk with the result from the analytic expression (equation 2).

4. FITTING PROCEDURE

Prior to the fitting of the adopted model to the observed lightcurves, a preliminary analysis of each lightcurve was performed. This was done to produce a set of initial parameters as a starting point for the fitting process. The orbital period can easily be estimated by measuring the average length of time between eclipses. Then, a coarse removal of the pulsation contribution to the lightcurve is achieved by phasing the data to the orbital period and fitting hyperbolas to both the primary and secondary eclipses. The out-of-eclipse flux is assumed to be 1.0. The result is an averaged lightcurve which gives clearly defined estimates for the average minima of both eclipses and average phase of external contact. Values for the inclination, radii and relative luminosities were obtained using an algorithm from Riazi (1992): from the values for the system light, in two filters, at the eclipse minima, this algorithm gives the relative luminosities of the two stars as well as the ratio of radii. From these, and the approximate phase angle at external contact, the inclination and relative radii can be computed. These values are then improved by performing a fit to minimize χ^2 relative to a simplified model. Once the boundaries of the eclipses have been defined the parameters controlling the Cepheid variability can be estimated by examining only the out-of-eclipse data. The pulsation period is found using a routine `period` from Press et al. (1992) on the out-of-eclipse data points. This routine uses an algorithm by Lomb (1976) to compute the power present at various frequencies in unevenly spaced data. Once the pulsation period is known, the data outside of eclipse can be phased to it and a Fourier series fit to the flux variation. The initial radial variation is simply set to be one quarter of the radius of the variable star and the offset is set to be one quarter of a period later than the time zeropoint for the lightcurve. The parameter set resulting from the above procedures will not accurately describe the lightcurve but it is usually sufficient to produce a lightcurve close enough to that observed to allow fitting to proceed and to be in the same valley in χ^2 parameter space as the global minimum.

The data are then subjected to a χ^2 minimization by means of a standard Levenberg-Marquandt method from Press et al. (1992). This procedure alternates between two complementary methods for finding a minimum χ^2: the steepest descent method far from the minimum, switching smoothly to the inverse Hessian method as the minimum is approached. This approach combines the advantages of both methods: rapid progress is made towards a minimum and, once located, accurate determination of the best-fit parameters is achieved. The drawback is the possibility of termination within a local minimum rather than the true minimum. This possibility can be reduced through reasonable selection of the initial values for the fitting process and examination of the final parameter set. An array of flags allows each parameter to be fit or held fixed. The data from both filters (or all three filters, when available) are fit simultaneously, allowing parameters such as the inclination and the radii,

which correspond to physical dimensions of the system (and so should not vary from filter to filter) to be determined from all of the data.

The limb-darkening coefficients prove to be the parameters most difficult to fit and have to be treated separately. A fit is first performed with all limb-darkening coefficients held fixed at their initial values, usually 0.5, to produce improved values for the other parameters. Another fit is then performed with the limb-darkening coefficients allowed to vary to produce optimum values for all parameters. The x will not vary far from 0.5, typically staying within 0.4 - 0.7, the range expected for x of most main-sequence and giant stars. The relative movement of the x_λ values can then be examined to see if it matches expectations based on the relative temperatures and surface gravities of the two stars. In practice the uncertainties on the limb-darkening coefficients prove to be too large for meaningful analysis. More "in eclipse" data would improve the constraints on these coefficients.

To distinguish between primary-variable and secondary-variable configurations, we solved for the system parameters with either configuration in turn. The set with the lower χ^2 was adopted.

We also investigated the possibility of sources of flux in each system in addition to the two eclipsing components. This involved assuming a third light source, of various brightnesss and refitting the system. In each of the three systems this produced no significant improvement in the fit.

5. RESULTS AND DISCUSSION

The best fit parameters for each of the systems are shown in Tables 9-11. The orbital and pulsational periods are both in days and the inclination is given in degrees. The radii (R) and amplitude of the radial variation (ΔR_{amp}) are relative to the orbital separation of the two stars. ΔR_{shift}, which measures the shift of the radial change relative to the temperature change, has units of days. Only the ratio of surface brightnesses J_V/J_R is tabulated as it was the only one that was fit directly and the other surface brightnesses are computed from it as outlined above. The limb-darkening coefficients, x_λ are as defined in equation 1. Once the relative surface brightness and radius of each star has been determined they can be combined with the mean system magnitude to compute the magnitude of each star in all filters. Also computed for each of the three Cepheids is the value of $W_R = R - 4.0(V - R)$, an index which corrects for most of the effects of reddening and effective temperature differences.

Figures 1-3 show the primary eclipses for each system along with the best fit lightcurve. Figure 4 shows a period-W_R diagram (P-L diagram) for MACHO Cepheids and the locations

of the three Cepheids studied here. This diagram is essentially free of reddening and allows us to classify the three Cepheids under study based on their relation to other LMC Cepheids without an explicit correction for extinction. The uncertainty ranges in the magnitude values in Tables 9-11 and Figure 4 were estimated from the range of possible component magnitudes based on the uncertainties in the best fit parameters. These are statistical uncertainties and likely underestimate the true uncertainties.

The colors and magnitudes of each star allow some general comments on the evolutionary state of each system if we assume each star follows a standard, single-star evolutionary history. This assumption is not unwarranted here given the large orbital periods of the systems. First, a crude correction for extinction must be made. To account for foreground reddening values of $E(B-V)$ are adopted from the map of Galactic foreground color excess toward the LMC published by Schwering & Israel (1991). This yields values of $E(B-V)$ for the three systems as follows: 0.08 for 6.6454.5, 0.08 for 78.6338.24 and 0.10 for 81.8997.87. These allow us to determine values for A_V and A_R when combined with the standard value of the ratio of total to selective extinction, $R_V = A_V/E(B-V) = 3.1$ (Cousins 1980), and $A_R/A_V = 0.77$ for our Cousins R and V from the interstellar extinction relations of Cardelli, Clayton, & Mathis (1989).

This procedure is clearly sufficient for the system 78.6338.24, producing $V_\circ = 16.20 \pm 0.03$ which agrees with the period-M_v relation of Alcock et al. (1998) for type II stars with log $P > 1.1$. Applying the correction described above to the system 81.8997.87 fails to produce V and R magnitudes for the Cepheid that are consistent with those expected of an overtone Cepheid of its period. Given the system's proximity to the 30 Doradus star-forming region it is not unreasonable to expect substantial extinction along this line of sight within the LMC and the closest Cepheid on the same plate, the overtone 81.8997.128, also appears well below the overtone band in the P-L diagram prior to applying a reddening correction. The period-magnitude relation for overtone Cepheids of Baraffe & Alibert (2001) gives $V_\circ = 15.86$ for the Cepheid in 81.8997.87, implying $A_v = 1.31$, a total value of $E(B-V) = 0.42$ and $R_\circ = 15.56$. Both $V_\circ$ and $R_\circ$ are consistent with the overtone bands in the period-V magnitude and period-R magnitude plots for MACHO LMC Cepheids. A total value of $E(B-V) = 0.41$ was obtained by de Marchi et al. (1993) for selected regions of 30 Doradus.

A further correction may also be necessary for the system 6.6454.5, however, the ambiguity in the classification of the Cepheid (see below) precludes definitively comparing its properties to those expected from a period-luminosity relation as was done with the other two systems. In light of this we adopt only the correction for foreground reddening.

After correction for reddening the values of V and $V-R$ are converted to the $L-T_{eff}$

plane by assuming $\mu_{LMC} = 18.5$ mag and using

$$log(T_{eff}) = 4.199 - \sqrt{0.08369 + 0.3493(V - R)} \tag{10}$$

a transformation of the Chiosi, Wood, & Capitanio (1993) semi-empirical calibration. Figures 5 and 6 show theoretical isochrones representative of the metallicities of Type I and Type II stellar populations: Y=0.25, Z=0.008 isochrones from Bertelli et al. (1994) in Figure 5 and Y=0.230, Z=0.0004 isochrones from Fagotto, Bressan, Bertelli, & Chiosi (1994) in Figure 6, along with the properties of the three systems. The error bars are computed exclusively from the errors in the magnitudes and colors given in Tables 9-11.

Based on the properties tabulated in Table 9 the system 6.6454.5 is found to contain a Cepheid as the secondary with a brighter, bluer primary. The nature of the Cepheid is unclear as its location in the P-L diagram (Figure 4) places it between the Type I and Type II bands, inconsistent with both classifications. The large amplitude of the radial variation, 0.323 ± 0.008 of the Cepheid's minimum radius is more consistent with a Type II classification. Fundamental-mode Type I Cepheids have typical radial variations of of 10% or less (Armstrong et al. 2001) while Type II Cepheids show larger radial excursions in the range of 30-50% of the minimum radius (Lebre & Gillet 1992).

If the Cepheid is assumed to be a Type II Cepheid it is either making an excursion from the AGB or moving off the HB to the AGB (a less likely scenario given its period). The companion, displayed in Figure 6, which also appears to be considerably evolved, is too luminous to fit either of these scenarios. It is possible that this system is not in the LMC but is instead a foreground object. A reduction in the assumed distance to the system to 17.8 kpc is necessary to shift the Cepheid's properties to fit a post-HB evolutionary state. By contrast, if the system is compared to Type I isochrones (Figure 5) the Cepheid's location is consistent with that expected but the companion appears to be too blue to fit the isochrones. If the Cepheid is indeed Type I, an additional reddening correction would need to be applied to make its location in Figure 4 consistent with the fundamental, Type I band. This would imply an even higher effective temperature and luminosity for the companion.

The status of 78.6338.24 is less ambiguous. It consists of a Type II Cepheid secondary with a hotter, but somewhat dimmer primary. With a pulsational period in excess of 17.5 days the Cepheid would classified as a W Vir type, which is consistent with its large radius relative to its companion and with its location in the P-L diagram (Figure 4). This system presented several challenges to modelling. The pulsation period of the Cepheid was found to not be constant over the duration of the observations. Despite being very small in magnitude (less than 1% of the period) this drift in period produced a substantial decrease in the quality of the fit. It was corrected to some degree by assuming a pulsational angular frequency that

was a slowly varying fuction of time, parameterized by:

$$\omega = \omega_\circ + A_1 Bt + A_2 (Bt)^2 \tag{11}$$

where the A_i are parameters to be determined by fitting and B is a constant, set by trial and error, to ensure that the A_i are of the same order as the other parameters. Inspection of the complete set of residuals after fitting revealed indications of non-sphericity in one (or both) of the system components. Both the asphericity and the "period drift" are consistent with the large radius and tenuous outer envelope of a W Vir star. Their locations in Figure 6 show both components to be well-evolved, post-HB or post-AGB objects.

The binary 81.8997.87 is distinct from the other two systems in several ways. Its variable is an intermediate-mass Cepheid pulsating in the first-overtone mode. Furthermore, the Cepheid is the primary with a considerably cooler, dimmer companion. The amplitude of radial pulsations is low, 0.060 ± 0.006 of the minimum Cepheid radius, as expected for an overtone Cepheid. Gieren (1982) provides an explicit determination of the radial displacement for the galactic overtone Cepheid SU Cas. The radial amplitude of that star is 0.026 of the mean Cepheid radius, similar to the value we find for 81.8997.87 (note that workers tend to avoid Baade-Wesslink analyses of overtone Cepheids due to the small dynamic range of the observables). Table 5a of Pel (1978) lists physical properties derived from fitting model atmospheres to the continuum colors of a sample of Galactic Cepheids. The values of $\Delta R/\langle R \rangle$ obtained for the six overtones in the sample range from 0.042 to 0.080. Once photometric contamination from the companion is removed the Cepheid's lightcurve shape, parameterized by the Fourier ratio R_{21}, is consistent with those of other MACHO overtone Cepheids of similar period. Its location in the P-L diagram (Figure 4) further reinforces this view. The companion's properties suggest a RGB star, possibly K class or later, however this combination of binary components is in poor agreement with current models of single star evolution. This is reflected in the disagreement with the isochrones seen in Figure 5. Indeed any system consisting only of these two stars may be evolutionarily inconsistent.

The observational coverage of this system is far from ideal. The 800-day orbital period limits the number of primary eclipses in the MACHO database to only 3. Furthermore the secondary eclipses appear to be non-existent. This can be accounted for by assuming a very low surface brightness for the secondary which will produce a very shallow secondary eclipse that could be dwarfed by the Cepheid variability. The absence of significant secondary eclipses could be a consequence of poor observational coverage. The near 2-day pulsational period (2.03 days) combined with MACHO's single-point per night coverage results in repeated sampling of the same two pulsation phases during an individual eclipse. These factors, poor coverage and the ill-defined secondary eclipses, produce large uncertainties in the fit parameters and component properties in Table 11 and Figure 4.

In these eclipsing systems, the radial displacement of the Cepheid can be detected directly solely from modelling of the photometric lightcurve. This is in contrast to most measurements of radial amplitude which are inferred from radial velocity measurements. As a test, the fits of all three systems were repeated with the amplitude of the radial displacement held fixed at 0 and the resulting χ^2 values compared to those with radial variation included. For the system 6.6454.5, χ^2_ν increased to 4.0, a 145% increase over the value of 1.6 listed in Table 9. For 81.8997.87 χ^2_ν increased to 1.5, an increase of only 26% over the best fit value of 1.1. For 78.6338.24 χ^2 increased to 8.8 from 7.5, only a 17% change. For each of the systems the change in χ^2 is found to be statistically significant for the number of degrees of freedom present. The relatively smaller impact of the radial amplitude on the quality of the fit for 78.6338.24 could be explained by at least two factors:

1. In this system the eclipse duration and pulsation timescales are sufficiently similar that they produce a degeneracy in a parameter set which includes ΔR.

2. The χ^2 value for this system is already elevated due to the model inadequacies previously mentioned. Their impact on the fit could easily dwarf the effects of the inclusion of radial amplitude.

For 81.8997.87 the small fractional amplitude of the radial change ($\sim$6%) could make its effect on the lightcurve difficult to discern.

6. SUMMARY AND FUTURE WORK

We have analysed the available multicolor photometry for three eclipsing Cepheids. The principal results of this work are:

1. MACHO Project V and R photometry for these important systems is reported.

2. The characterization of the three systems using a self-consistent eclipsing binary lightcurve model which includes the effects of radius and surface brightness change due to the pulsating star.

3. The interpretation of the evolutionary state of the three systems, with two of the three systems conforming poorly to the expectations from standard, single star evolutionary theory.

4. Direct evidence of radial size change in a Cepheid variable. To date, this has been implied (apparently correctly!) by integrating the radial velocity curves of Cepheids.

Michelson interferometry is capable of measuring the angular diameters of Cepheids but to date the change in angular diameter, which is direct evidence for radius change, has only been reported for a single Cepheid (Lane et al. 2000).

5. The prediction of future primary and secondary eclipses and their fine structure to facilitate follow-up observations (see below).

6. The identification of the factors which limit the usefulness of the lightcurve model which has been developed.

Follow-up photometric observations are clearly warranted for all of these systems, but especially for 81.8997.87 which is clearly an intermediate-mass, first-overtone Cepheid. Indeed, several of us have obtained multicolor photometry of the April 2001 primary minimum of this system using the 74-inch telescope at Mount Stromlo Observatory, Canberra, Australia. More densely spaced observations of this system during a future secondary minimum, especially longer wavelength photometry, are likely to provide significantly improved values for surface brightness ratios. To facilitate future observations predicted dates of primary and secondary minima are listed for all three systems in Tables 12-14.

The full impact of the discovery of eclipsing Cepheids in the LMC will only be realized when radial velocity curves for both components in each system have been obtained. Recently, Cycle 10 HST (Hubble Space Telecope) observations were taken by a collaboration involving several coauthors on this paper and led by Edward Guinan of Villanova University. For 81.8997.87, it appears that spectral observations in the far red will be necessary to improve the contrast of the secondary stars spectral lines relative to the Cepheid. The long orbital periods of these systems imply numerous HST visits over the course of approximately a year to map out the radial velocity curves completely. Fortunately, the relatively small amplitude of the radial velocity curve of the Cepheid will result in a clean separation of the orbital and pulsation components with a small number of visits.

We are very grateful for the skilled support given our project by the technical staff at the Mount Stromlo Observatory, and in particular we would like to thank Simon Chan, Glen Thorpe, Susannah Sabine, and Michael McDonald for their invaluable assistance in obtaining the data. This work was performed under the auspices of the U.S. Department of Energy by the University of California, Lawrence Livermore National Laboratory under contract No. W-7405-Eng-48. Work performed by the Center for Particle Astrophysics personnel is supported in part by the Office of Science and Technology Centers of the NSF under cooperative agreement A-8809616. Work performed at MSSSO is supported by the Bilateral Science and Technology Program of the Australian Department of Industry, Technology and Regional Development. DM is supported by FONDAP. D. L. W. and D. Lepischak were

supported in part by a Research Grant from the Natural Sciences and Engineering Research Council of Canada (NSERC) during this work. This work comprised part of the M.Sc. thesis of D. Lepischak.

REFERENCES

Alcock, C. et al. 1999, PASP, 111, 1539

Alcock, C. et al. 1998, AJ, 115, 1921

Alcock, C. et al. 1995, AJ, 109, 1653

Armstrong, J. T., Nordgren, T. E., Germain, M. E., Hajian, A. R., Hindsley, R. B., Hummel, C. A., Mozurkewich, D., & Thessin, R. N. 2001, AJ, 121, 476

Baraffe, I. & Alibert, Y. 2001, A&A, 371, 592

Barnes, T. G., Evans, D. S., & Parsons, S. B. 1976, MNRAS, 174, 503

Bell, R. A. & Gustafsson, B. 1980, MNRAS, 191, 435

Bertelli, G., Bressan, A., Chiosi, C., Fagotto, F., & Nasi, E. 1994, A&AS, 106, 275

Binnendijk, L. 1960, Properties of Double Stars, Philadelphia : University of Pennsylvania Press, 1960.

Cardelli, J. A., Clayton, G. C., & Mathis, J. S. 1989, ApJ, 345, 245

Chiosi, C., Wood, P. R., & Capitanio, N. 1993, ApJS, 86, 541

Cousins, A. W. J. 1980, South African Astronomical Observatory Circular, 1, 234

de Marchi, G., Nota, A., Leitherer, C., Ragazzoni, R., & Barbieri, C. 1993, ApJ, 419, 658

Fagotto, F., Bressan, A., Bertelli, G., & Chiosi, C. 1994, A&AS, 104, 365

Fernie, J. D. & Evans, N. R. 1997, PASP, 109, 541

Gieren, W. 1982, PASP, 94, 960

Harris, H. C., Olszewski, E. W., & Wallerstein, G. 1984, AJ, 89, 119

Lane, B. F., Kuchner, M. J., Boden, A. F., Creech-Eakman, M., & Kulkarni, S. R. 2000, Nature, 407, 485

Lebre, A. & Gillet, D. 1992, A&A, 255, 221

Lomb, N. 1976, Astrophysics and Space Science, 39, 447–462.

Nelson, B. & Davis, W. D. 1972, ApJ, 174, 617

Pel, J. W. 1978, A&A, 62, 75

Press, W. H., Teukolsky, S. A., Vetterling, W. T., & Flannery, B. P. 1992, Numerical Recipies in C, Cambridge: University Press, 1992, 2nd ed.,

Riazi, N. 1992, AJ, 104, 228

Rodríguez, E. & Breger, M. 2001, A&A, 366, 178

Rodríguez, E., Claret, A., Sedano, J. L., Garcia, J. M., & Garrido, R. 1998, A&A, 340, 196

Schechter, P. L., Mateo, M., & Saha, A. 1993, PASP, 105, 1342

Schwering, P. B. W. & Israel, F. P. 1991, A&A, 246, 231

Thiessen, G. 1956, Zeitschrift Astrophysics, 39, 65

Udalski, A., Soszyński, I., Szymański, M., Kubiak, M., Pietrzyński, G., Woźniak, P., & Żebruń, K. 1999, Acta Astronomica, 49, 223

Table 1. V Photometry for 6.6454.5

HJD	V *(mag)*	σ_V *(mag)*	Source
2449074.95500	14.6530	0.0150	MACHO
2449075.06470	14.6520	0.0150	MACHO
2449075.96150	14.6840	0.0150	MACHO
2449076.99790	14.7080	0.0150	MACHO
2449077.11200	14.7190	0.0150	MACHO
2449081.02760	14.7020	0.0150	MACHO
2449082.99210	14.6240	0.0160	MACHO
2449083.94080	14.6240	0.0160	MACHO
2449084.97280	14.6290	0.0150	MACHO
2449085.94290	14.6740	0.0160	MACHO
2449088.06740	14.6020	0.0150	MACHO
2449088.96770	14.6030	0.0150	MACHO
2449089.97160	14.6390	0.0150	MACHO
2449093.90660	14.5990	0.0150	MACHO
2449098.04000	14.6050	0.0150	MACHO

Table 2. R Photometry for 6.6454.5

HJD	R *(mag)*	σ_R *(mag)*	Source
2448824.17260	14.5560	0.0160	MACHO
2448827.18660	14.5590	0.0150	MACHO
2448829.14130	14.5420	0.0160	MACHO
2448830.15910	14.5260	0.0150	MACHO
2448833.15680	14.6010	0.0150	MACHO
2448834.27580	14.5370	0.0150	MACHO
2448835.14270	14.4810	0.0150	MACHO
2448836.21040	14.5340	0.0150	MACHO
2448837.13050	14.5520	0.0150	MACHO
2448843.16980	14.6000	0.0160	MACHO
2448844.13490	14.5380	0.0150	MACHO
2448851.15840	14.5840	0.0150	MACHO
2448854.28290	14.5080	0.0160	MACHO
2448855.25190	14.5290	0.0150	MACHO
2448857.30420	14.6080	0.0150	MACHO

Table 3. I Photometry for 6.6454.5

HJD	I *(mag)*	σ_I *(mag)*	Source
2450832.78089	14.4520	0.0080	OGLE
2450834.74339	14.3600	0.0150	OGLE
2450836.68017	14.4310	0.0140	OGLE
2450838.75705	14.3800	0.0100	OGLE
2450839.71152	14.3690	0.0100	OGLE
2450840.69671	14.3890	0.0070	OGLE
2450841.77146	14.4440	0.0060	OGLE
2450842.69221	14.4470	0.0110	OGLE
2450843.69775	14.3800	0.0100	OGLE
2450844.69179	14.3490	0.0070	OGLE
2450845.55570	14.3901	0.0079	CTIO
2450845.80135	14.3850	0.0080	OGLE
2450846.75718	14.4380	0.0070	OGLE
2450850.73583	14.3890	0.0110	OGLE
2450851.65660	14.4245	0.0079	CTIO

Table 4. V Photometry for 78.6338.24

HJD	V *(mag)*	σ_V *(mag)*	Source
2448886.25480	15.5390	0.0150	MACHO
2448888.15230	15.6790	0.0170	MACHO
2448889.20710	15.6940	0.0160	MACHO
2448893.23740	15.8760	0.0170	MACHO
2448895.21320	16.0230	0.0190	MACHO
2448896.18200	16.1130	0.0160	MACHO
2448897.24090	16.0870	0.0170	MACHO
2448902.27770	15.5770	0.0150	MACHO
2448917.16550	15.8170	0.0160	MACHO
2448919.19520	15.4720	0.0150	MACHO
2448924.20640	15.6990	0.0150	MACHO
2448933.25020	16.0810	0.0240	MACHO
2448940.15000	15.6570	0.0160	MACHO
2448942.17400	15.7230	0.0160	MACHO
2448949.13640	16.1180	0.0160	MACHO

Table 5. R Photometry for 78.6338.24

HJD	R *(mag)*	σ_R *(mag)*	Source
2448886.25480	15.2120	0.0150	MACHO
2448888.15230	15.3130	0.0170	MACHO
2448889.20710	15.3140	0.0160	MACHO
2448893.23740	15.4970	0.0170	MACHO
2448895.21320	15.6400	0.0180	MACHO
2448896.18200	15.7300	0.0150	MACHO
2448897.24090	15.7460	0.0170	MACHO
2448902.27770	15.2600	0.0150	MACHO
2448917.16550	15.5060	0.0160	MACHO
2448919.19520	15.1810	0.0150	MACHO
2448924.20640	15.3400	0.0150	MACHO
2448933.25020	15.7500	0.0270	MACHO
2448940.15000	15.2980	0.0160	MACHO
2448942.17400	15.3340	0.0160	MACHO
2448949.13640	15.7660	0.0150	MACHO

Table 6. V Photometry for 81.8997.87

HJD	V *(mag)*	σ_V *(mag)*	Source
2448919.24260	17.1530	0.0220	MACHO
2448920.04760	17.0300	0.0230	MACHO
2448921.04080	17.1880	0.0220	MACHO
2448924.25670	16.9930	0.0230	MACHO
2448927.99640	16.9700	0.0270	MACHO
2448929.03000	17.1960	0.0200	MACHO
2448929.97740	16.9830	0.0240	MACHO
2448930.97620	17.1670	0.0360	MACHO
2448931.99100	17.0060	0.0240	MACHO
2448932.16440	16.9770	0.0240	MACHO
2448934.13420	16.9560	0.0220	MACHO
2448936.13460	16.9940	0.0420	MACHO
2448938.18980	16.9860	0.0300	MACHO
2448939.01450	17.1340	0.0280	MACHO
2448940.03150	17.0110	0.0240	MACHO

Table 7. R Photometry for 81.8997.87

HJD	R *(mag)*	σ_R *(mag)*	Source
2448919.24260	16.4420	0.0170	MACHO
2448920.04760	16.3470	0.0180	MACHO
2448921.04080	16.4710	0.0170	MACHO
2448924.25670	16.3450	0.0180	MACHO
2448927.99640	16.3040	0.0190	MACHO
2448929.03000	16.4600	0.0170	MACHO
2448929.97740	16.3200	0.0180	MACHO
2448930.97620	16.4390	0.0210	MACHO
2448931.99100	16.3390	0.0180	MACHO
2448932.16440	16.3170	0.0180	MACHO
2448934.13420	16.2960	0.0170	MACHO
2448936.13460	16.3140	0.0240	MACHO
2448938.18980	16.3100	0.0210	MACHO
2448939.01450	16.4250	0.0190	MACHO
2448940.03150	16.3440	0.0180	MACHO

Table 8. I Photometry for 81.8997.87

HJD	I *(mag)*	σ_I *(mag)*	Source
2450739.86067	15.6720	0.0100	OGLE
2450744.76901	15.7840	0.0130	OGLE
2450745.85362	15.6680	0.0130	OGLE
2450746.83950	15.7950	0.0180	OGLE
2450747.73495	15.6580	0.0130	OGLE
2450750.79988	15.8020	0.0130	OGLE
2450751.80069	15.6610	0.0200	OGLE
2450752.85852	15.7830	0.0110	OGLE
2450755.78274	15.6530	0.0100	OGLE
2450759.70861	15.6680	0.0150	OGLE
2450761.78982	15.6860	0.0130	OGLE
2450766.83954	15.7490	0.0150	OGLE
2450773.79513	15.7050	0.0140	OGLE
2450776.82033	15.7410	0.0140	OGLE
2450778.85342	15.7100	0.0100	OGLE

Table 9. Best fit parameters for 6.6454.5. Meanings of individual parameters and units are explained in the text.

χ^2_v	1.6		
P_{orb} (d)	397.142 ± 0.005		
i $(^\circ)$	86.71 ± 0.04		
Companion	(primary)	Variable	(secondary)
R	0.0522 ± 0.0004	R_{min}	0.051 ± 0.001
$\frac{J_V}{J_R}$	1.061 ± 0.002	$<\frac{J_V}{J_R}>$	0.748 ± 0.005
x_V	0.46 ± 0.17	x_V	0.52 ± 0.85
x_R	0.48 ± 0.20	x_R	0.42 ± 0.72
x_I	0.45 ± 0.18	x_I	0.56 ± 0.55
		P_{ceph} (d)	4.97371 ± 0.00002
		ΔR_{amp}	0.0166 ± 0.0002
		ΔR_{shift} (d)	-0.17 ± 0.01
Intensity-weighted Mean Magnitudes and Colours			
V	14.82 ± 0.04	$<V>$	16.7±0.1
R	14.80 ± 0.04	$<R>$	16.3± 0.1
I	14.72 ± 0.04	$<I>$	15.89± 0.09
$V-R$	0.018 ± 0.002	$<V-R>$	0.452 ± 0.007
$V-I$	0.102± 0.003	$<V-I>$	0.81± 0.01
		$<W_R>$	14.4±0.1

Table 10. Best fit parameters for 78.6338.24. Parameter definitions and units are the same as in Table 9 with the exception of A_1 and A_2 which are defined by equation 11.

χ^2_v	7.5		
P_{orb} (d)	419.718 ± 0.008		
i $(^\circ)$	86.94 ± 0.02		
Companion	(primary)	Variable	(secondary)
R	0.0403 ± 0.0002	R_{min}	0.0717 ± 0.0004
$\frac{J_V}{J_R}$	1.146 ± 0.001	$<\frac{J_V}{J_R}>$	0.9118 ± 0.001
x_V	0.46 ± 0.17	x_V	0.52 ± 0.85
x_R	0.48 ± 0.20	x_R	0.42 ± 0.72
		P_{ceph} (d)	17.68586 ± 0.0003
		A_1	2.265 ± 0.007
		A_2 (d)	-448 ± 2
		ΔR_{amp}	0.03106 ± 0.0002
		ΔR_{shift} (d)	-6.07 ± 0.01
Intensity-weighted Mean Magnitudes and Colours			
V	16.55 ± 0.02	$<V>$	16.20±0.03
R	16.35 ± 0.02	$<R>$	15.75± 0.03
$V-R$	0.20 ± 0.03	$<V-R>$	0.447 ± 0.001
		$<W_R>$	13.98±0.03

Table 11. Best-fit parameters for 81.8997.87. Parameters are the same as in Table 9. The large uncertainties in the limb-darkening coefficients of the secondary indicate that while these parameters are allowed to vary, they are essentially unmodified and unconstrained by the lightcurve. The tabulated x_λ are the original values and the errors are included for consistency.

χ^2_v	1.2		
P_{orb} (d)	800.5 ± 0.1		
i $(^\circ)$	87.0 ± 0.2		
Variable	(primary)	Companion	(secondary)
R_{min}	0.029± 0.001	R	0.047 ± 0.005
$< \frac{J_V}{J_R} >$	1.078 ± 0.009	$\frac{J_V}{J_R}$	0.54 ± 0.05
x_V	0.50 ± 0.94	x_V	0.50 ± 6.06
x_R	0.50 ± 0.91	x_R	0.50 ± 4.52
x_I	0.50 ± 0.98	x_I	0.50 ± 3.02
P_{ceph} (d)	2.035321 ± 0.000009		
ΔR_{amp}	0.0017 ± 0.0002		
ΔR_{shift} (d)	0.21 ± 0.01		
Intensity-weighted Mean Magnitudes and Colours			
$< V >$	17.2 ± 0.2	V	20±1
$< R >$	16.6 ± 0.2	R	19.2± 0.9
$< I >$	16.0 ± 0.2	I	17.9± 0.8
$< V - R >$	0.602 ± 0.009	$V - R$	1.3± 0.1
$< V - I >$	1.137± 0.007	$V - I$	2.6± 0.2
$< W_R >$	14.1±0.2		

Table 12. Predicted dates of future eclipses for 6.6454.5.

Primary Eclipse		Secondary Eclipse	
JD	UT	JD	UT
2452454.78	2002 Jun 28 18.79	2452653.37	2003 Jan 13 8.80
2452851.95	2003 Jul 30 22.80	2453050.53	2004 Feb 14 12.80
2453249.12	2004 Aug 31 2.80	2453447.70	2005 Mar 17 16.81
2453646.28	2005 Oct 2 6.81	2453844.87	2006 Apr 18 20.81
2454043.45	2006 Nov 3 10.81	2454242.03	2007 May 21 0.82
2454440.62	2007 Dec 5 14.82	2454639.20	2008 Jun 21 4.82
2454837.78	2009 Jan 5 18.82	2455036.37	2009 Jul 23 8.83
2455234.95	2010 Feb 6 22.83	2455433.53	2010 Aug 24 12.83
2455632.12	2011 Mar 11 2.83	2455830.70	2011 Sep 25 16.84

Table 13. Predicted dates of future eclipses for 78.6338.24.

Primary Eclipse		Secondary Eclipse	
JD	UT	JD	UT
2452379.74	2002 Apr 14 17.70	2452589.47	2002 Nov 10 11.29
2452799.20	2003 Jun 8 4.88	2453008.94	2004 Jan 3 22.48
2453218.67	2004 Jul 31 16.07	2453428.40	2005 Feb 26 9.66
2453638.14	2005 Sep 24 3.25	2453847.87	2006 Apr 21 20.84
2454057.60	2006 Nov 17 14.43	2454267.33	2007 Jun 15 8.02
2454477.07	2008 Jan 11 1.61	2454686.80	2008 Aug 7 19.20
2454896.53	2009 Mar 5 12.79	2455106.27	2009 Oct 1 6.39
2455316.00	2010 Apr 28 23.98	2455525.73	2010 Nov 24 17.57
2455735.46	2011 Jun 22 11.16	2455945.20	2012 Jan 18 4.75

Table 14. Predicted dates of future eclipses for 81.8997.87.

Primary Eclipse		Secondary Eclipse	
JD	UT	JD	UT
2452010.81	2001 Apr 10 19.47	2452411.27	2002 May 16 6.45
2452811.73	2003 Jun 20 17.44	2453212.18	2004 Jul 25 4.42
2453612.64	2005 Aug 29 15.40	2454013.10	2006 Oct 4 2.38
2454413.56	2007 Nov 8 13.37	2454814.01	2008 Dec 13 0.35
2455214.47	2010 Jan 17 11.33	2455614.93	2011 Feb 21 22.32
2456015.39	2012 Mar 28 9.30	2456415.85	2013 May 2 20.28
2456816.30	2014 Jun 7 7.26	2457216.76	2015 Jul 12 18.25
2457617.22	2016 Aug 16 5.23	2458017.68	2017 Sep 20 16.21
2458418.13	2018 Oct 26 3.20	2458818.59	2019 Nov 30 14.18
2459219.05	2021 Jan 4 1.16	2459619.51	2022 Feb 8 12.14

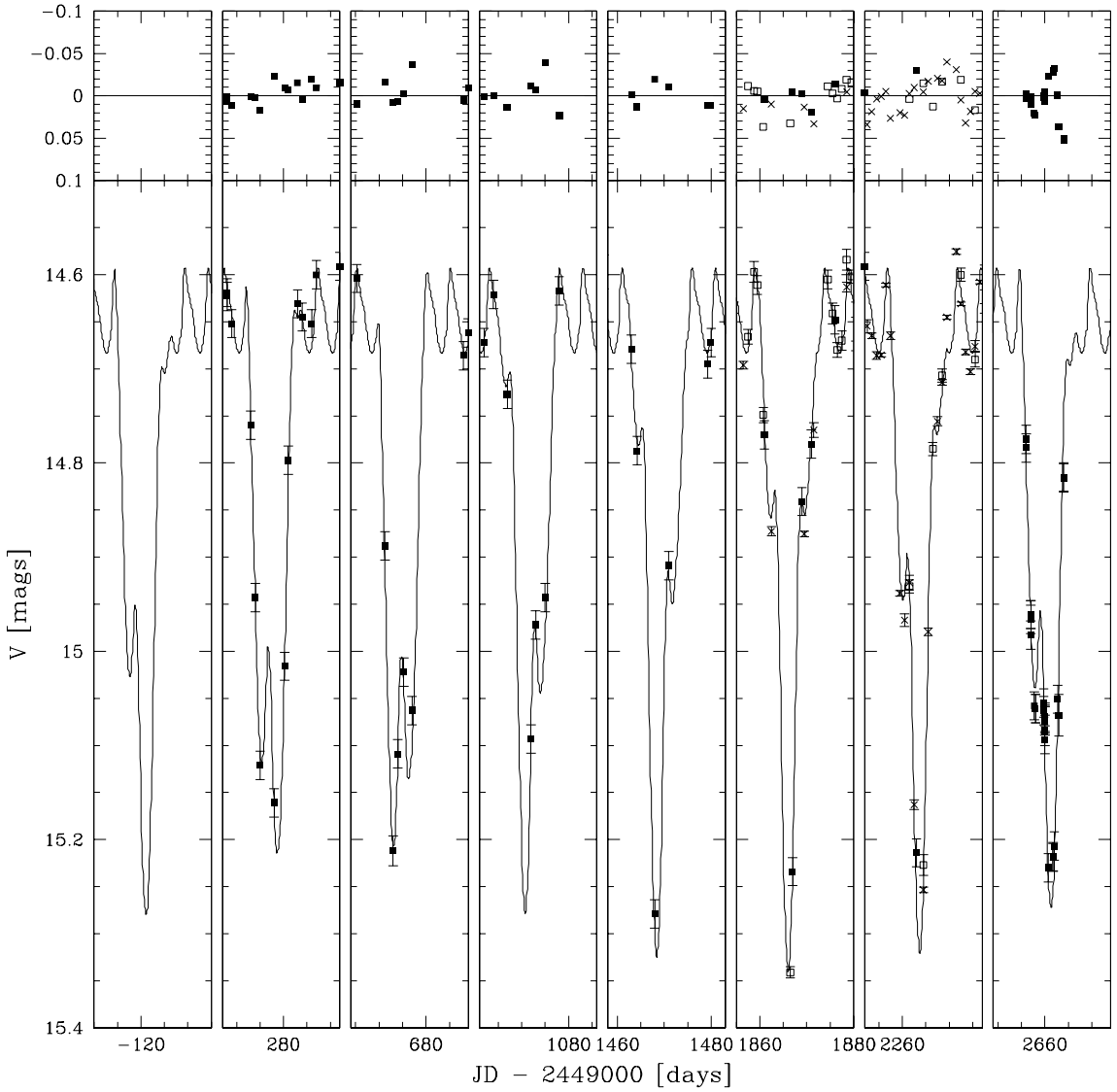

Fig. 1.— Primary eclipses of 6.6454.4 in V with curve of best fit. Upper panels show residuals in magnitudes. Filled boxes indicate observations from the MACHO project, open boxes indicate observations from the OGLE project, x's are follow-up observations taken at CTIO.

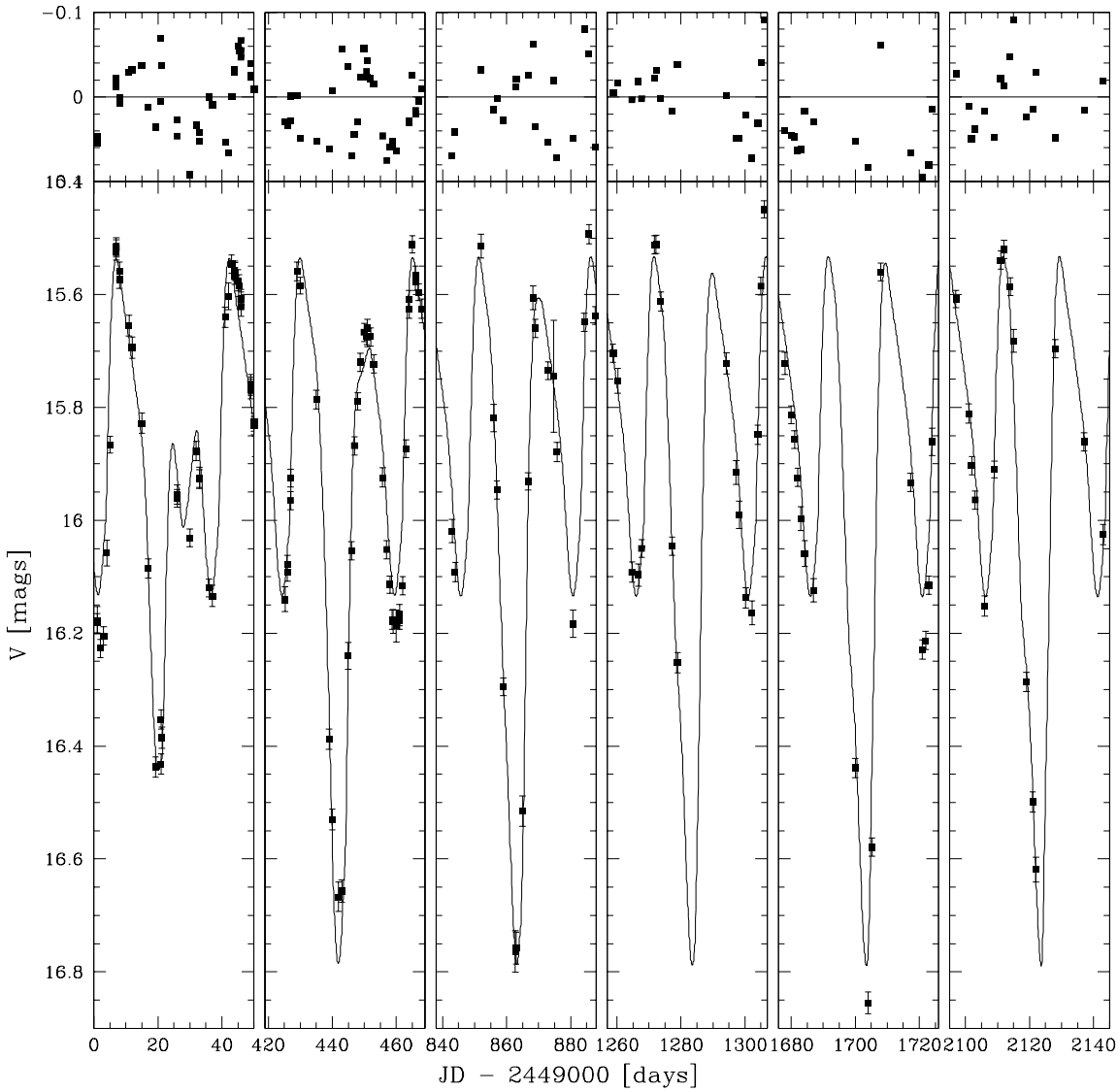

Fig. 2.— Primary eclipses of 78.6338.24 in V with curve of best fit. Upper panels show residuals in magnitudes. All points are from the MACHO project database.

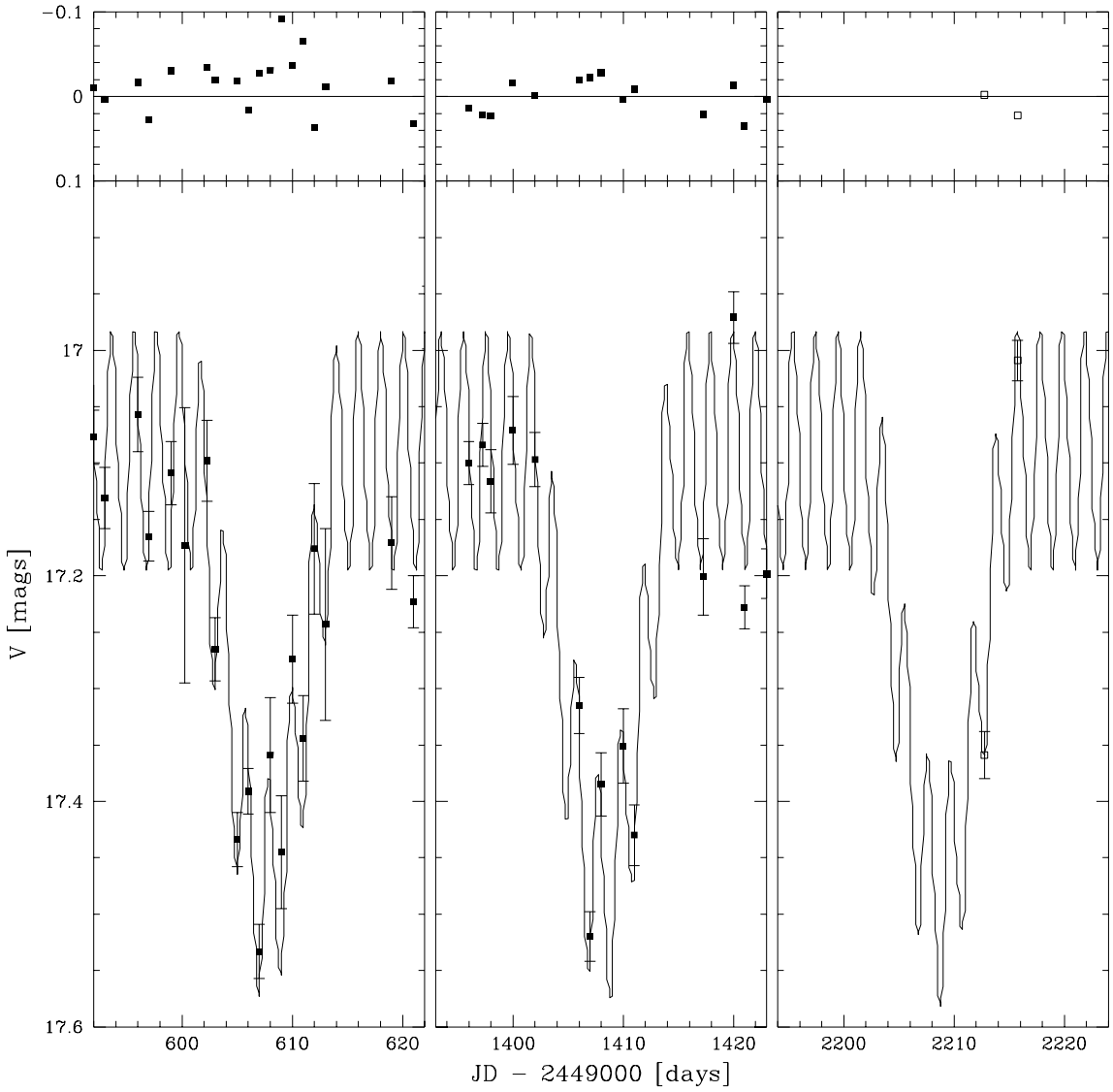

Fig. 3.— Primary eclipses of 81.8997.87 in V with curve of best fit. Upper panels show residuals in magnitudes. Filled boxes indicate observations from the MACHO project, open boxes observations from the OGLE project.

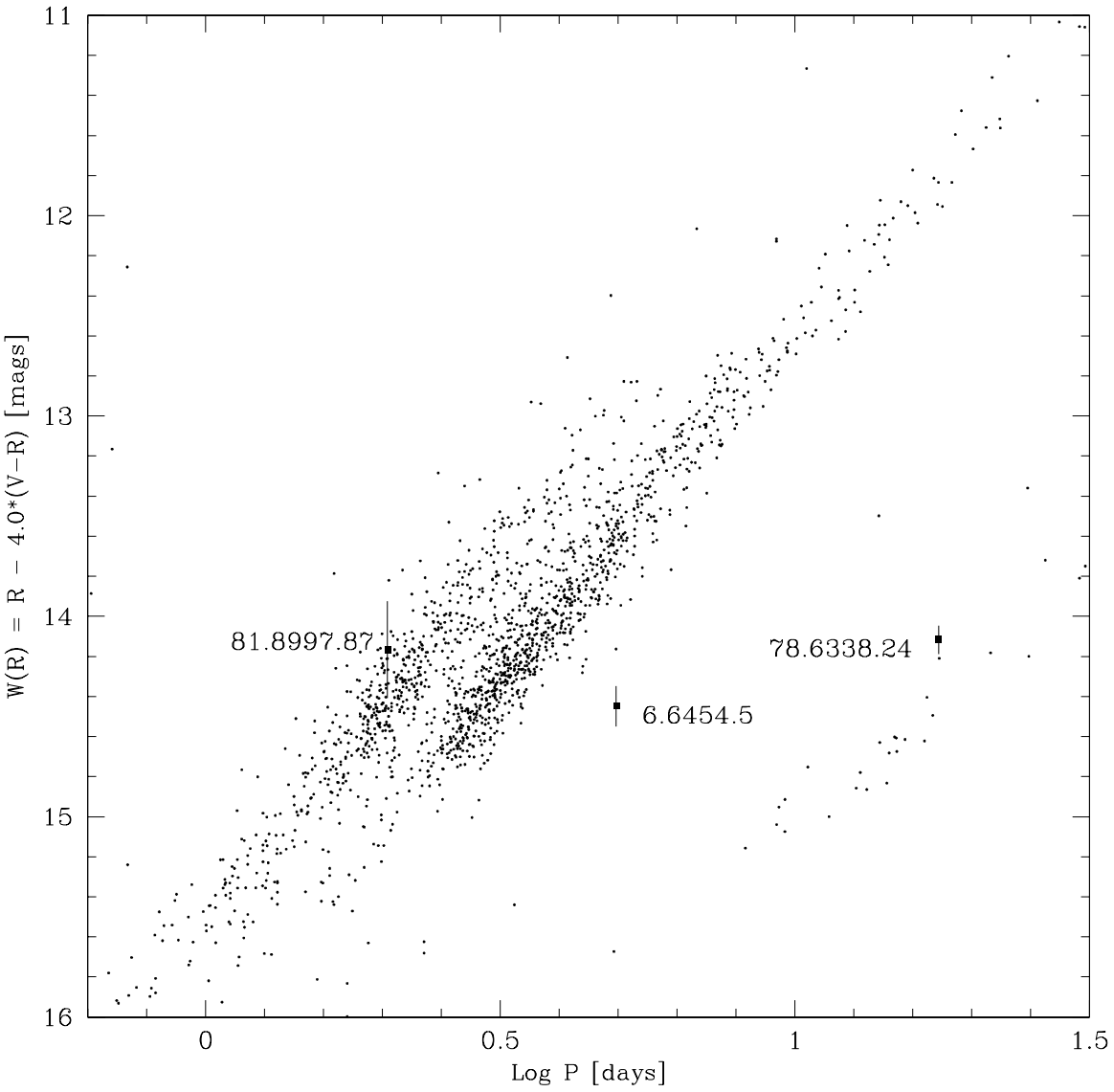

Fig. 4.— W_R vs. $log_{10}P$ diagram for 1766 MACHO Cepheids. The brighter sequence at a given period are Cepheids pulsating in the first overtone and the sequence extending to longer periods are fundamental mode pulsators. Stars in the lower right are Type II Cepheids. The locations of the three Cepheids studied here are indicated. Their magnitudes and colors are from the best-fit parameters and thus have had the companion flux removed.

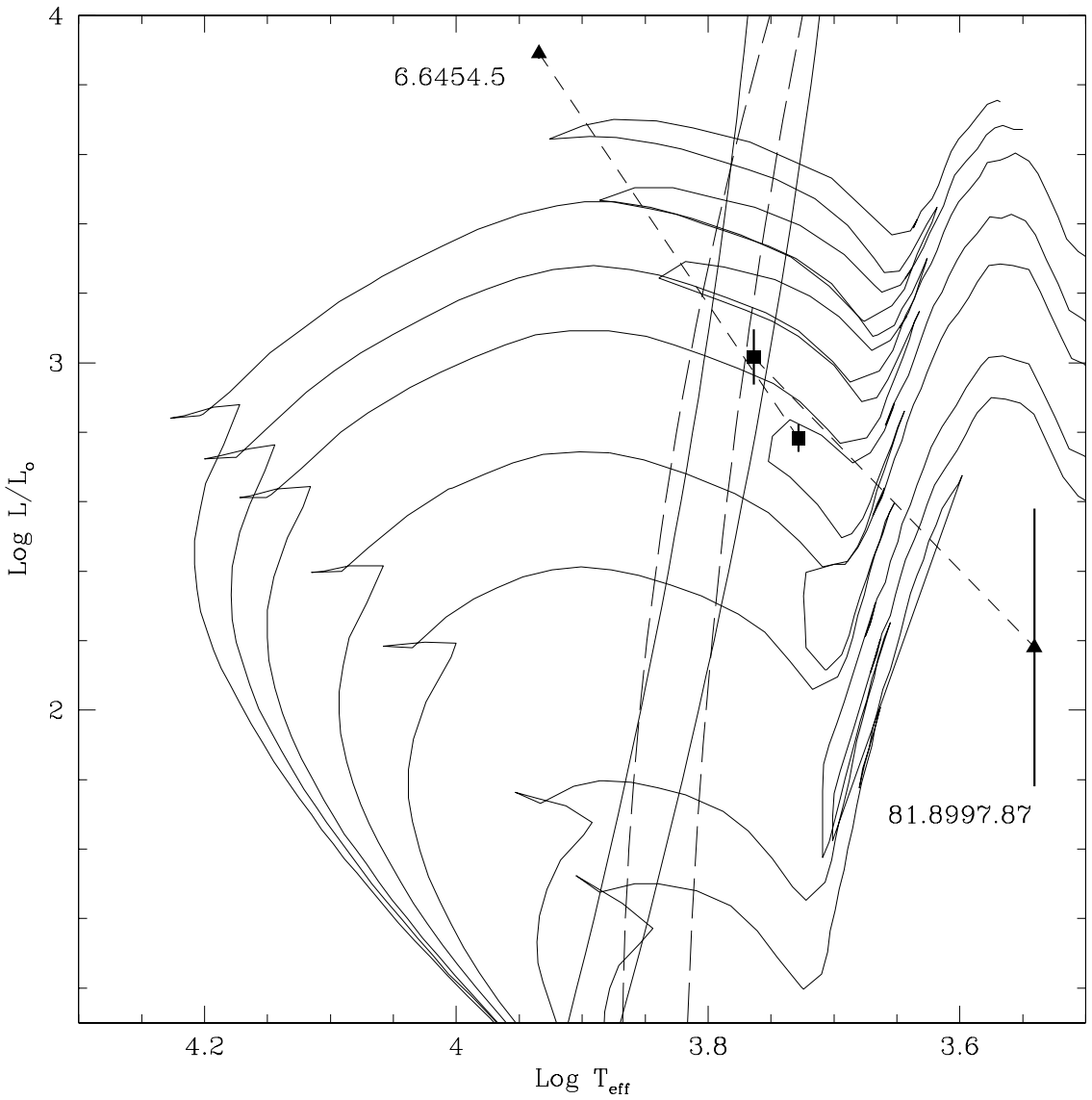

Fig. 5.— Systems 6.6454.5 and 81.8997.87 compared with theoretical isochrones for Y = 0.25, Z = 0.008 stars (Bertelli et al. 1994) ranging from log(age)=9.1 to log(age)=7.9 [years]. Also shown are the theoretical fundamental (solid) and overtone (dashed) instability strips of Chiosi, Wood, & Capitanio (1993). Cepheids are shown as solid squares, their companions as solid triangles. Dashed lines connect system members.

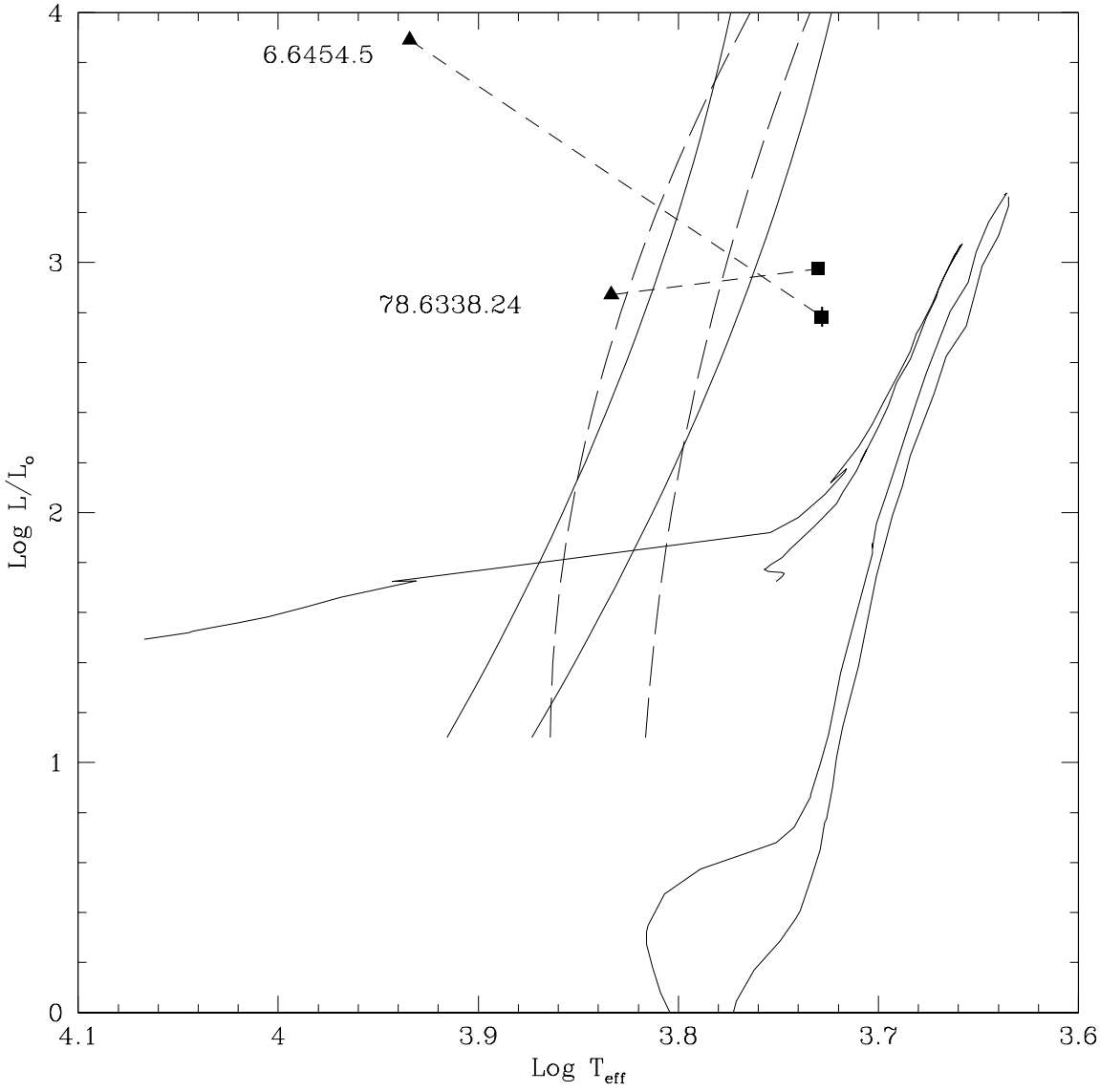

Fig. 6.— Systems 6.6454.5 and 78.6338.24 compared with theoretical isochrones for Y = 0.230, Z = 0.0004 stars (Fagotto, Bressan, Bertelli, & Chiosi 1994). Also shown are the theoretical fundamental (solid) and overtone (dashed) instability strips of Chiosi, Wood, & Capitanio (1993).